Xu et al. Respiratory Research (2025) 26:137
https://doi.org/10.1186/s12931-025-03206-9

Respiratory Research

RESEARCH Open Access

A nomogram model based on clinical and 3D-EIT parameters for CTEPH diagnosis

Jian Xu[1†], Yuhan Wang[2†], Ying Gong[1,3†], Lu Wang[1], Yuanlin Song[1,2,3,4,5*] and Xu Wu[1,3*]

Abstract

Background Chronic thromboembolic pulmonary hypertension (CTEPH) is easily misdiagnosed. Three-dimensional (3D) electrical impedance tomography (EIT) can monitor the whole-lung perfusion at the bedside. In this study, three-dimensional electrical impedance tomography (3D-EIT) features in patients with suspected chronic thromboembolic pulmonary hypertension (CTEPH) was investigated, and nomogram models based on clinical and 3D-EIT parameters were constructed to identify CTEPH.

Methods Patients with pulmonary hypertension (PH) due to left heart disease and chronic hypoxia were excluded. The enrolled patients were divided into CTEPH and Non-CTEPH groups by confirmatory tests. Then, history and laboratory results were collected and 3D-EIT examination was performed. Out of 70 enrolled patients, 50 cases were used as the training set to construct the nomogram model. Obtained nomogram diagnostic model was calibrated and then evaluated using receiver operating characteristic (ROC) curves, decision curve analysis (DCA), and clinical impact curves (CIC).

Results Through a comprehensive univariate analysis, Wald test, Akaike information criterion (AIC), and Bayesian information criterion (BIC), the nomogram model for CTEPH diagnosis based on 50 patients was constructed using venous thromboembolism (VTE) history, D-dimer, maximum of corresponding regional ventilation/perfusion ratio (V/Qmax), range between the maximum and minimum values of regional perfusion (P-Range) and the percentage of ventilation/perfusion match area (VQMatch). The C-index of the nomogram model in the training set was 0.926 (95% CI: 0.859–0.993). In the training set and test set, the nomogram model had a larger area under the curve (AUC) than models containing only VTE history, VTE history + D-dimer and EIT parameters. Both DCA and CIC analyses indicate that this model can provide significant clinical benefits.

Conclusions A nomogram model combining clinical and 3D-EIT parameters facilitated the diagnosis of CTEPH.

Clinical trial number Not applicable.

Keywords Chronic thromboembolic pulmonary hypertension (CTEPH), Electrical impedance tomography (EIT), Nomogram, Diagnosis

†Jian Xu, Yuhan Wang and Ying Gong contributed equally to this work.

*Correspondence:
Yuanlin Song
ylsong70@163.com
Xu Wu
wu.xu@zs-hospital.sh.cn

Full list of author information is available at the end of the article

Background

Chronic thromboembolic pulmonary hypertension (CTEPH) is categorized as group four pulmonary hypertension (PH) according to the guidelines by the European Society of Cardiology and the European Respiratory Society (ESC/ERS). CTEPH is associated with a challenging prognosis; without treatment, individuals with a mean pulmonary artery pressure (mPAP) above 40 mmHg have only a 30% chance of surviving beyond five years [1]. Although CTEPH leads to high morbidity and mortality, it remains frequently underdiagnosed. This is attributed to several factors, including the nonspecific nature of its symptoms and the limitations of accessible imaging modalities, which make it challenging to accurately identify at-risk individuals [2, 3].

Electrical impedance tomography (EIT) is gaining recognition as a radiation-free imaging technique, enabling non-invasive, real-time bedside monitoring of regional lung ventilation, and potentially perfusion, particularly for patients in intensive care [4, 5]. EIT-derived assessments of ventilation and perfusion offer a unique combination of functional and anatomical insights [6]. Growing evidence supports the use of EIT to evaluate regional lung perfusion, particularly in conditions like pulmonary embolism (PE) [7] and acute respiratory distress syndrome (ARDS) [8, 9]. In the context of pulmonary vascular diseases, electrical impedance tomography (EIT) offers a complementary approach to traditional hemodynamic assessments [10], providing insights into changes in pulmonary artery pressure [11]. This technique shows promise for estimating lung perfusion and monitoring patients with PH. Clinical studies have highlighted the diagnostic potential of EIT, particularly when used in conjunction with hypertonic saline bolus injections [12]. EIT has demonstrated high reliability in visualizing perfusion, suggesting its potential as an alternative to computed tomography pulmonary angiography (CTPA) [13]. A recent advancement in EIT technology involves a pulsatility-based method designed to quantify perfusion signals. This approach enables the calculation of the percentage of matched or unmatched ventilation-perfusion regions, allowing for a completely non-invasive evaluation of perfusion [14]. Additionally, the development of three-dimensional EIT (3D-EIT) has enabled comprehensive whole-lung ventilation and perfusion assessment, effectively identifying perfusion deficits that earlier two-dimensional methods could overlook. However, comparative studies examining the use of EIT in patients with pulmonary vascular diseases like CTEPH remain limited.

This study aimed to develop a more straightforward approach for identifying CTEPH in patients with PH by utilizing 3D-EIT parameters alongside readily available clinical indicators. Various statistical methods were employed to select significant variables, and a nomogram was constructed to integrate clinical characteristics and 3D-EIT metrics, forming a diagnostic model for CTEPH.

Methods

Study design and participants

This prospective study was conducted at Zhongshan Hospital in Shanghai, China, from 2021 to 2023, with approval from Zhongshan Hospital's ethics committee (Approval No. 402) in accordance with the Declaration of Helsinki. Written informed consent was obtained from all participants. All included patients were hospitalized in the respiratory ward. All patients were unscheduled and came to the hospital on their own for treatment of certain symptoms. Patients presenting with features of PH were included, provided they were not classified under category II or III causes of PH based on diagnostic and treatment guidelines from the European Society of Cardiology and European Respiratory Society. However, for the mPAP criterion, we adopted the Chinese guideline (mPAP ≥ 25 mmHg) to better align with the population under study. PH diagnosis was confirmed via right heart catheterization or, for patients unable to tolerate catheterization or unwilling to undergo an invasive examination, echocardiography. Participants were then categorized into CTEPH and Non-CTEPH groups based on the presence or absence of perfusion deficits observed through V/Q scanning or CTPA.

Participants were excluded if they had not undergone V/Q scanning or CTPA within one week or if their mean pulmonary artery pressure was below 25 mmHg. Additional exclusion criteria included age under 18 years, a body mass index exceeding 40 kg/m², ribcage deformities, or any contraindications to the use of EIT, such as pregnancy, chest injuries that prevented electrode belt placement, or the presence of automatic implantable cardioverter defibrillators or implantable pumps. Clinical histories and laboratory data were collected on the day of enrollment. The enrollment process is illustrated in Fig. 1.

EIT-based ventilation and perfusion measurement

All enrolled patients underwent EIT measurements while spontaneously breathing in the supine position. Two EIT belts, each containing 16 surface electrodes, were positioned around the thorax at the armpit and xiphoid levels. EIT data were acquired using the Infivision 1900 Impedance Imaging System (Infivision Medical Imaging Technology Co., Ltd.) and processed through digital filtering methods, as described in prior studies.

The image reconstruction was achieved through a deep generative model-integrated three-dimensional (3D) time-difference imaging algorithm, implemented using Python and TensorFlow. The algorithm takes as input the difference between two frames of data and outputs

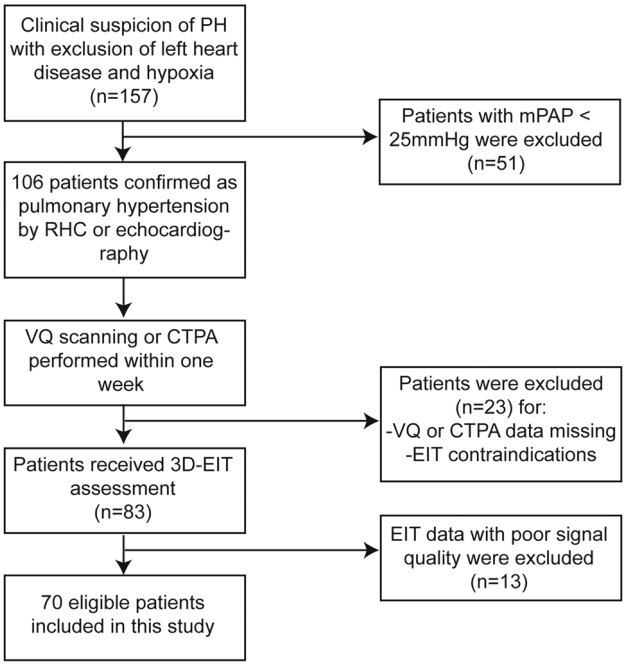

Fig. 1 Flow diagram of patient enrollment

a reconstructed 3D image that reflects the conductivity changes in the chest between the two time points. For ventilation imaging, one frame is selected from the ventilation-related signal at the end of expiration, and the other from the end of inspiration. For perfusion imaging, one frame is selected from the cardiac-related signal at the end of systole, and the other from the end of diastole. In the reconstructed ventilation (or perfusion) image, the ventilated (or perfused) region is defined as pixels whose amplitude exceeds 35% of the maximum pixel amplitude in the image. It is important to note that the heart region is excluded from the perfused area, as the heart and lungs exhibit opposite conductivity changes during perfusion.

Both the ventilation and perfusion maps were divided into six cross quadrants: lower left (LL), lower right (LR), middle left (ML), middle right (MR), upper left (UL), and upper right (UR). Only the ventilated or perfused regions were considered for evaluation. The regional ventilation distribution (V, %), perfusion distribution (Q, %), and the ventilation-to-perfusion ratio (V/Q) were calculated for each quadrant (LL, LR, ML, MR, UL, and UR).

Further, the following three terms were defined: region that is only ventilated ($\mathrm{R_V}$), region that is only perfused ($\mathrm{R_P}$), and region that is both ventilated and perfused ($\mathrm{R_{V+P}}$). From the aspect of set theory, $\mathrm{R_V} = \text{ventilated region} - \text{perfused region}$, $\mathrm{R_P} = \text{perfused region} - \text{ventilated region}$, and $\mathrm{R_{V+P}} = \text{ventilated region} \cap \text{perfused region}$. The percentages of the three regions can be calculated as:

$$\text{DeadSpace } (\%) = \frac{\text{area of } \mathrm{R_V}}{\text{area of } \mathrm{R_V} + \text{area of } \mathrm{R_P} + \text{area of } \mathrm{R_{V+P}}} \times 100$$

$$\text{Shunt } (\%) = \frac{\text{area of } \mathrm{R_P}}{\text{area of } \mathrm{R_V} + \text{area of } \mathrm{R_P} + \text{area of } \mathrm{R_{V+P}}} \times 100$$

$$\text{VQMatch } (\%) = \frac{\text{area of } \mathrm{R_{V+P}}}{\text{area of } \mathrm{R_V} + \text{area of } \mathrm{R_P} + \text{area of } \mathrm{R_{V+P}}} \times 100$$

In addition, V/Qmax indicated the maximum value of the ventilation/perfusion ratio in the six lung regions (relative worst perfusion). P-Range (%) referred to range between the maximum and minimum values of regional perfusion.

Statistical analysis

Data analysis was conducted using R (version 4.3.3). Baseline data were examined with the CBCgrps package. T-tests were applied to continuous variables that followed a normal distribution, while the Wilcoxon rank-sum test was used for non-normally distributed data. The Chi-square test was employed for binary classification parameters. The rcorr package was used for correlation analysis between variables, and the circlize package was used to generate chord diagrams. A *P*-value of < 0.05 was considered statistically significant.

Training set partitioning and variable selection

The data were split into training and test sets with a 7:3 ratio using the createDataPartition function in the caret package in R. To ensure the balance of grouping conditions across the two datasets, stratified sampling based on grouping was employed. To assess differences between the variables in the two sets, the CBCgrps package was utilized. In the training set, univariate logistic regression was applied to identify variables associated with CTEPH, using the finalfit package. For the variables selected through univariate analysis, the Wald test, variance inflation factor (VIF) analysis, Akaike information criterion (AIC), and Bayesian information criterion (BIC) were comprehensively utilized to further refine and select variables for inclusion in the model. The car package was used to compute the VIF values, while the Wald test, AIC, and BIC were analyzed by R's built-in functions.

Nomogram model construction and evaluation

Selected variables were used to construct the nomogram model for CTEPH diagnosis with the rms and regplot packages. The Hmisc package was used to calculate the C-index of the nomogram model. Calibration analysis was performed on the training set using the rms package with the bootstrap value of 1000. Then, receiver operating characteristic (ROC) analyses of the nomogram model and models with clinical parameters or EIT parameters were performed using the training and test sets with the pROC package. What's more, decision curve

analysis (DCA) and clinical impact curves (CIC) analysis were used to evaluate the performance of the nomogram diagnostic model with the rmda package. Integrated discrimination improvement (IDI) analysis was employed to compare the incremental benefits brought by the model as parameters were added stepwise, using the PredictABEL package.

Results

Baseline characteristics of enrolled patients

During the study period, a total of 157 patients exhibiting characteristics suggestive of pulmonary hypertension (such as chest tightness, a history of pulmonary embolism, or previously documented elevated mean pulmonary artery pressure estimated by echocardiography) were screened. These patients were excluded if they had significant left heart disease or a history of chronic hypoxia; all others provided written informed consent. Of these, 106 patients confirmed to have pulmonary hypertension through right heart catheterization (RHC) or echocardiography (for patients who were clinically assessed as intolerant to RHC or unwilling to undergo invasive examinations) met the eligibility criteria for enrollment. However, 23 patients were excluded due to insufficient imaging data or contraindications to 3D-EIT. Finally, 13 patients were excluded due to 3D-EIT data with poor quality that did not meet the analytical requirements. As a result, 70 patients were included in the final analysis. The enrollment flow diagram is presented in Fig. 1.

After discriminating tests, including V/Q scanning and CTPA, the enrolled patients were categorized into two groups: CTEPH ($n = 37$) and Non-CTEPH ($n = 33$). Clinical data (e.g., age, gender, history of venous thromboembolism (VTE)), laboratory findings (e.g., D-dimer), echocardiography parameters (e.g., mPAP, the maximum value of tricuspid regurgitation velocity (TRV max), right atrial dimensions (RAD)) and 3D-EIT parameters (e.g., VQMatch, V/Qmax) were recorded for each patient. The distribution of baseline parameters between the two groups and the results of the statistical tests for differences are presented in Table 1. Notably, systolic pressure, PE history, deep venous thrombosis (DVT) history, VTE history, and D-dimer levels showed significant differences between the CTEPH and Non-CTEPH groups. The echocardiographic parameters showed no significant differences between the two groups. For 3D-EIT parameters, significant differences were observed in V/Qmax, DeadSpace VQMatch, and P-Range. To better understand the background of VTE, VTE-related etiological factors (e.g., immobility, injury, cancer) were collected and analyzed, but no significant statistical differences were observed between the two groups (Table S1). Additionally, the ventilation and perfusion measurements for each lung region obtained from 3D-EIT are presented in Table S2. Typical ventilation, perfusion, VQ matching images, and V/Q scanning images from one CTEPH patient are shown in Fig. 2. Based on SPECT perfusion imaging, this patient exhibited perfusion defects in the left lower segment, right upper segment, and right lower segment (Fig. 2A, B, and F). In parallel, the 3D-EIT images revealed a homogeneous ventilation distribution with a marked bilateral lower lung perfusion deficit (Fig. 2C, D, E, and F). Both lower lungs also displayed abnormally elevated V/Q ratios (Fig. 2G). Since RHC is the true gold standard for diagnosing PH, the patients who underwent RHC and those who did not among the 70 cases were compared and described separately. In the CTEPH group, 14 (37.84%) patients underwent RHC, while in the Non-CTEPH group, 12 (36.36%) patients underwent RHC, with no statistically significant difference in this ratio ($P = 1$). Additionally, the baseline characteristics of patients who underwent RHC and those who did not showed no significant differences in most variables (except for D-dimer and VQMatch) (Table S3). In summary, clinical and 3D-EIT parameters differed between the CTEPH and Non-CTEPH groups, and the 3D-EIT perfusion images effectively reflected lung perfusion defects.

Correlation analysis of variables

To assess the correlation between variables in the baseline data, Spearman's method was used to calculate the correlation coefficients and *P*-values. It is evident that there is a strong correlation among parameters related to EIT and among those derived from echocardiography (Fig. 3A). For instance, mPAPe and TRV max show a positive correlation ($r = 0.85$, $P < 0.01$), while DeadSpace and VQMatch exhibit a negative correlation (r = -0.65, $P < 0.01$). However, the correlations between clinical or echocardiography parameters and 3D-EIT parameters were relatively weak. The relationships between variables were visualized using a chord diagram (Fig. 3B). These findings suggest that integrating both clinical information and 3D-EIT results is a reasonable approach for diagnosing CTEPH.

Training set partitioning and variable filtering for model construction

To construct a nomogram model for CTEPH diagnosis, the data were randomly divided into training and test sets in a 7:3 ratio. A total of 50 patients were assigned to the training set, while 20 patients were assigned to the test set. Among the patients, 26 (52%) in the training set and 11 (55%) in the test set were diagnosed with CTEPH, with no statistically significant difference ($P = 1$) between the two sets. The distribution of each parameter in the training and test sets, along with the results of statistical

Table 1 Baseline characteristics of enrolled subjects

Variables	Total (*n* = 70)	Non-CTEPH (*n* = 33)	CTEPH (*n* = 37)	*P* value
Basic information and clinical parameters				
Gender				0.681
male	46 (65.71%)	23 (69.70%)	23 (62.16%)	
female	24 (34.29%)	10 (30.30%)	14 (37.84%)	
Age (yrs) †	60.1 ± 16.49	59.21 ± 16.22	60.89 ± 16.91	0.673
Heart rate (beats/min)	80.5 (78, 89.75)	81 (80, 89)	80 (76, 91)	0.475
Systolic pressure (mmHg)†	123.81 ± 18.11	118.12 ± 18.98	128.89 ± 15.88	0.013,*
SaO_2 (%)	97 (96,98)	98 (97,98)	97 (95,98)	0.074
Hemoptysis				0.434
No	63 (90.00%)	31 (93.94%)	32 (86.49%)	
Yes	7 (10.00%)	2 (6.06%)	5 (13.51%)	
Chest tightness				0.591
No	39 (55.71%)	20 (60.61%)	19 (51.35%)	
Yes	31 (44.29%)	13 (39.39%)	18 (48.65%)	
Palpitations				0.277
No	52 (74.29%)	27 (81.82%)	25 (67.57%)	
Yes	18 (25.71%)	6 (18.18%)	12 (32.43%)	
Leg swelling				0.171
No	58 (82.86%)	30 (90.91%)	28 (75.68%)	
Yes	12 (17.14%)	3 (9.09%)	9 (24.32%)	
Syncope				0.714
No	62 (88.57%)	30 (90.91%)	32 (86.49%)	
Yes	8 (11.43%)	3 (9.09%)	5 (13.51%)	
PE history				0.014,*
No	56 (80%)	31 (93.94%)	25 (67.57%)	
Yes	14 (20%)	2 (6.06%)	12 (32.43%)	
DVT history				0.001,**
No	47 (68.57%)	29 (87.88%)	18 (48.65%)	
Yes	23 (31.43%)	4 (12.12%)	19 (51.35%)	
VTE history				< 0.001,***
No	42 (60.00%)	28 (84.85%)	14 (37.84%)	
Yes	28 (40.00%)	5 (15.15%)	23 (62.16%)	
Right heart catheterization#				
mPAP (mmHg)	38 (28.25, 47)	38.5 (29.25, 53.75)	38 (28.25, 46.5)	0.68
CO (L/min/m2)	4.24 (3.28, 5.53)	4.5 (3.58, 5.44)	3.72 (3.26, 5.63)	0.631
Laboratory parameters				
D-dimer (mg/L)	0.83 (0.37, 3.61)	0.6 (0.35, 1.01)	1.67 (0.38, 7.06)	0.030,*
cTnT (μg/L)	0.01 (0.01, 0.02)	0.01 (0.01, 0.02)	0.02 (0.01, 0.03)	0.133
NT-proBNP (pg/mL)	440.5 (205.75, 1230)	459 (212, 1057)	422 (205, 1421)	0.916
Echocardiography parameters				
mPAPe (mmHg)	57.5 (48, 70.75)	63 (49, 76)	54 (45, 64)	0.144
TRV max (cm/s)	441.5 (400, 492)	467 (409, 511)	433 (389, 467)	0.178
RADs-long diameter (mm)	48 (45.25, 51)	48 (46, 52)	48 (45, 50)	0.781
RADs-short diameter (mm)	42 (40, 44.75)	41 (40, 45	42 (40, 44)	0.53
Pericardial effusion				1
No	65 (92.86%)	31 (93.94%)	34 (91.89%)	
Yes	5 (7.14%)	2 (6.06%)	3 (8.11%)	
EIT parameters				
V/Qmax	3.01 (2.23, 6.4)	2.83 (2.05, 3.6)	4.48 (2.46, 9.78)	0.003,**
DeadSpace (%)	28.18 (25.36, 33.2)	26.72 (23.72, 31.95)	29.69 (26.74, 35.34)	0.017,*
Shunt (%)	4.83 (2.06, 9.05)	4.37 (1.79, 6.63)	5.91 (2.73, 10.48)	0.096

Table 1 (continued)

Variables	Total ($n = 70$)	Non-CTEPH ($n = 33$)	CTEPH ($n = 37$)	*P* value
VQMatch (%)	65.87 (61.55, 69.9)	69.29 (65.45, 72.46)	62.89 (60.72, 67.04)	< 0.001,***
P-Range (%)	26.72 (24.15, 32.57)	25.11 (22.01, 26.8)	29.95 (25.53, 34.11)	0.002,**

A total of 26 (37.14%) patients underwent right heart catheterization, 14 (37.84%) in the CTEPH group and 12 (36.36%) in the Non-CTEPH group, with no statistical differences ($P = 1$) (Table S3)

Data are displayed as mean ± standard deviation if the continuous variable conforms to a normal distribution, otherwise as median (lower quartile, upper quartile). Categorical variables are presented as n%. †, normal distribution; *, $P < 0.05$; **, $P < 0.01$; ***, $P < 0.001$

Abbreviations: SaO_2, arterial oxygen saturation; PE, pulmonary embolism; DVT, deep venous thrombosis; VTE, venous thromboembolism; mPAP, mean right pulmonary artery pressure; CO, cardiac output; cTnT, cardiac troponin T; NT-pro BNP, N-terminal pro-brain natriuretic peptide; mPAPe, mPAP on echocardiography; TRV max: the maximum value of tricuspid regurgitation velocity; RAD, right atrial dimension; EIT, electrical impedance tomography; V, ventilation; Q, perfusion; V/Qmax: relative maximum of corresponding regional ventilation/perfusion ratio; DeadSpace, the area of dead space detected by EIT; Shunt, the area of shunt detected by EIT; VQMatch, the area with matched ventilation and perfusion on EIT; P-Range: range between the maximum and minimum values of regional perfusion

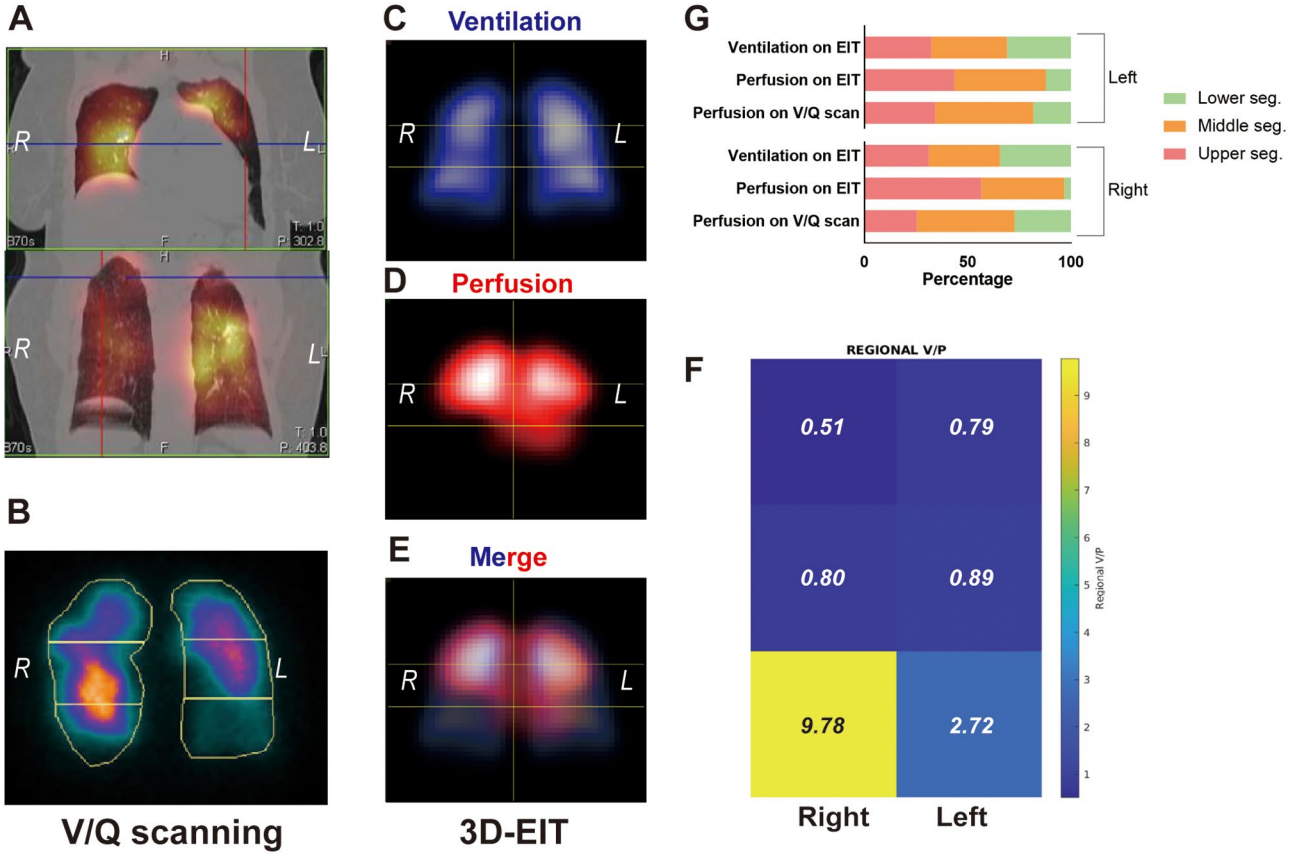

Fig. 2 Typical V/Q scanning and 3D-EIT images of patients in the CTEPH group. (**A**) The perfusion scanning images merged with coronal CT reconstructed images. (**B**) The total perfusion-related radioactivity on VQ scanning in the supine anterior position. (**C**) The ventilation image derived from 3D-EIT. The brightness of the blue color represents the level of ventilation. (**D**) The perfusion image derived from 3D-EIT. The brightness of the red color represents the level of perfusion. (**E**) A merged image of the EIT ventilation image and perfusion image. (**F**) Stacked histograms of the percentage of ventilation or perfusion in 6 lung regions named before on EIT and SPECT. (**G**) The ventilation-perfusion ratios (V/Q) of each lung region

tests for differences, is presented in Table S4. Except for some 3D-EIT-derived parameters, no significant differences were observed in the parameters between the training and test sets. Therefore, this data partitioning method was deemed suitable for constructing and testing the subsequent nomogram model.

To select variables for model construction, univariate logistic regression analyses were conducted on individual clinical and EIT parameters in the training set. Parameters related to right heart catheterization, such as mPAP and cardiac output (CO), were excluded from the analysis, as the goal was to identify easily accessible, non-invasive diagnostic markers. The univariate analysis revealed that the following variables were statistically significant ($P < 0.05$ and the confidence interval did not intersect the invalid line): PE history, DVT history, VTE history, D-dimer, V/Qmax, DeadSpace, VQMatch, and P-Range, which included both clinical and 3D-EIT

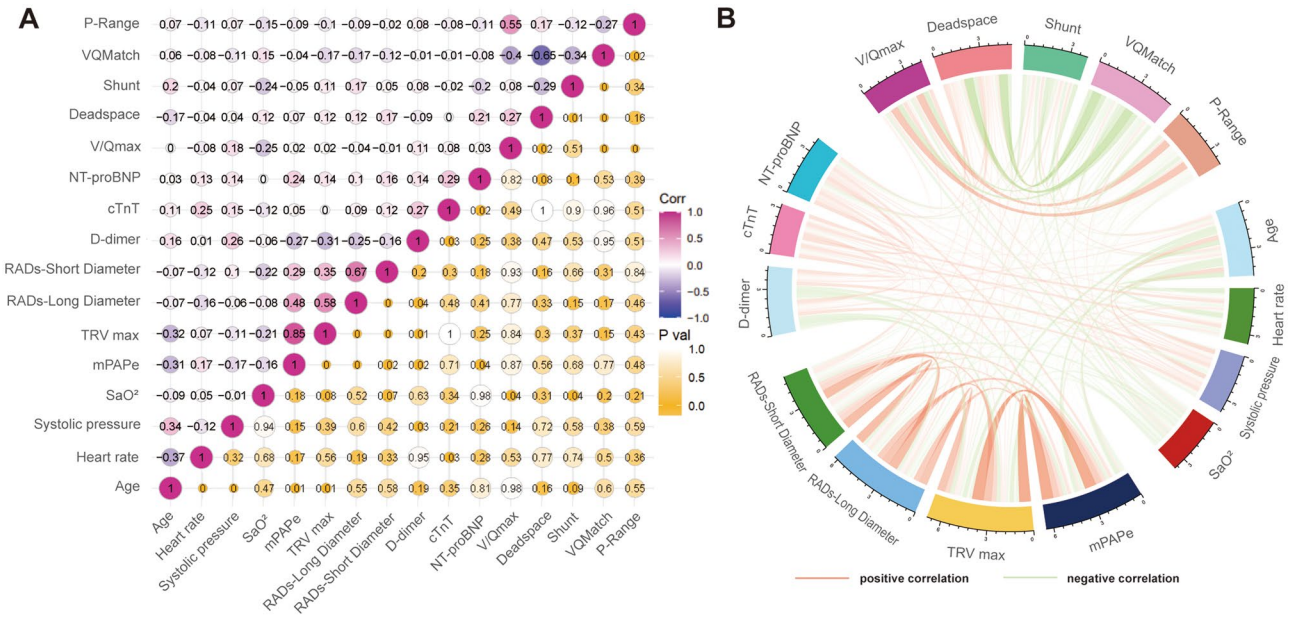

Fig. 3 Variable correlation analysis. (**A**) Correlation coefficients and *P*-values between the variables. (**B**) The chord diagram showing the correlation of variables. The thickness of the chord represents the strength of the correlation. Red is for positive correlation and green is for negative correlation

parameters (Table 2). Subsequently, the Wald test was used to further refine the selection of parameters (Table S5). Only one parameter, D-dimer, showed significant difference ($P = 0.0359$). Therefore, the variables selected through univariate analysis were directly screened and included in the model based on clinical significance, VIF, AIC, and BIC. VIF analysis indicated that the medical history parameters and the EIT parameters DeadSpace and VQMatch may exhibit multicollinearity (Table 3). Considering clinical significance, the parameter VTE history was retained because it encompasses both PE and DVT cases and had a lower *P*-value in the univariate analysis. Regarding the EIT parameters, DeadSpace reflects the proportion of dead space ventilation associated with poor lung perfusion, while VQMatch represents the proportion of ventilation-perfusion matched regions. These two parameters were individually included in models (Model 2 and Model 3 in Table 3) for evaluation. Based on a comprehensive analysis of VIF, AIC, and BIC, all variables in Model 3 had VIF values below 10, and the model overall demonstrated lower AIC and BIC values, making it the superior model. Therefore, the subsequent nomogram model incorporated the following parameters: VTE history, D-dimer, V/Qmax, VQMatch, and P-Range.

Nomogram model construction and evaluation

VTE history, D-dimer, V/Qmax, VQMatch, and P-Range were selected as variables for constructing the nomogram model in the training set. As examples, a typical CTEPH patient had a high total score and predictive probability in the model, while a Non-CTEPH patient had a low total score and predictive probability (Fig. 4A and B). The C-index of the nomogram in the training set was 0.926 (95% CI: 0.859–0.993). Next, the model was calibrated using the bootstrap method. The calibration curve analysis indicated that the predicted probabilities closely matched the actual observed probabilities, with a mean absolute error of only 0.046 (Fig. 4C).

To further assess the diagnostic performance of the model, various analyses were conducted using the test set. ROC analysis showed that the area under the curve (AUC) for the nomogram model (0.9263 in the training set and 0.8990 in the test set) was higher than those of VTE history (0.7420 in the training set and 0.7273 in the test set), VTE history + D-dimer model (0.7716 in the training set and 0.8586 in the test set) and the EIT-parameter model with V/Qmax, VQMatch and P-Range (0.8109 in the training set and 0.7172 in the test set) (Fig. 5A and B). Additionally, IDI analysis was applied to calculate the incremental benefits brought by the model as variables were added stepwise. In the training set, the nomogram model provided incremental benefits compared to models that included only VTE history (IDI: 0.333), VTE history + D-dimer (IDI: 0.2539), and EIT parameters (IDI: 0.2776), and these improvements were statistically significant (Table S6). Also, the model combining VTE history and D-dimer outperformed the model with VTE history alone. However, in the test set, the IDI among models with different parameters did not show significant differences. This may be due to the small sample size of the test set, resulting in limited evaluation

Table 2 Univariate logistic regression analyses for differentiating CTEPH

Variables	OR (with 95% CI)	*P* value
Gender	1.06 (0.33–3.47)	0.924
Age	1.01 (0.97–1.04)	0.738
Heart rate	0.99 (0.94–1.03)	0.518
Systolic pressure	1.02 (0.99–1.06)	0.229
SaO_2	0.83 (0.62–1.05)	0.145
Hemoptysis	1.43 (0.22–11.69)	0.707
Chest tightness	1.18 (0.39–3.64)	0.768
Palpitation	1.14 (0.30–4.56)	0.848
Leg swelling	4.05 (0.86–29.46)	0.104
Syncope	1.27 (0.25–7.11)	0.769
PE history	6.87 (1.55–48.89)	0.022,*
DVT history	6.82 (1.94–28.82)	0.005,*
VTE history	8.55 (2.50-33.97)	0.001,*
D-dimer	1.21 (1.05–1.53)	0.047,*
cTnT (-log10)	0.82 (0.19–3.43)	0.786
NT-proBNP	1.00 (1.00–1.00)	0.365
mPAPe	0.98 (0.95–1.01)	0.278
TRV max	1.00 (0.99-1.00)	0.257
RADs-Long Diameter	0.99 (0.88–1.12)	0.923
RADs-Short Diameter	1.07 (0.89–1.30)	0.488
Pericardial effusion	0.92 (0.10–8.18)	0.933
V/Qmax	1.26 (1.07–1.58)	0.021,*
DeadSpace (%)	1.09 (1.02–1.21)	0.04,*
Shunt (%)	1.11 (1.01–1.26)	0.059
VQMatch (%)	0.84 (0.73–0.95)	0.013,*
P-Range (%)	1.12 (1.03–1.24)	0.012,*

Each OR is displayed with its 95% CI. *, $P<0.05$ and the CI did not intersect the invalid line

Abbreviations: OR, odds ratio; CI, confidence interval; SaO_2, arterial oxygen saturation; PE, pulmonary embolism; DVT, deep venous thrombosis; VTE, venous thromboembolism; cTnT, cardiac troponin T; NT-pro BNP, N-terminal pro-brain natriuretic peptide; mPAPe, mean pulmonary arterial pressure on echocardiography; TRV max: the maximum value of tricuspid regurgitation velocity; RAD, right atrial dimensions; V, ventilation; Q, perfusion; V/Qmax: relative maximum of corresponding regional ventilation/perfusion ratio; DeadSpace, the area of dead space detected by EIT; Shunt, the area of shunt detected by EIT; VQMatch, the area with matched ventilation and perfusion on EIT; P-Range: range between the maximum and minimum values of regional perfusion

Table 3 Analysis of VIF, AIC, and BIC for the model derived from univariate regression analysis

	Variables	VIF value	AIC	BIC
Model 1	PE history	2.247562	50.0875	67.2957
	DVT history	6.938138		
	VTE history	10.291355		
	D-dimer	1.295521		
	V/Qmax	1.838151		
	DeadSpace (%)	8.636968		
	VQMatch (%)	7.988679		
	P-Range (%	2.027614		
Model 2	VTE history	1.079233	49.4344	60.90654
	D-dimer	1.14003		
	V/Qmax	1.231658		
	DeadSpace (%)	1.087897		
	P-Range (%)	1.348481		
Model 3 (Nomogram)	VTE history	1.050144	46.7734	58.24553
	D-dimer	1.26664		
	V/Qmax	1.228703		
	VQMatch (%)	1.145556		
	P-Range (%)	1.430455		

Abbreviations: VIF, Variance inflation factor; AIC, Akaike information criterion; BIC: Bayesian information criterion; PE, pulmonary embolism; DVT, deep venous thrombosis; VTE, venous thromboembolism; V/Qmax: relative maximum of corresponding regional ventilation/perfusion ratio; DeadSpace, the area of dead space detected by EIT; VQMatch, the area with matched ventilation and perfusion on EIT; P-Range: range between the maximum and minimum values of regional perfusion

power. Nonetheless, the IDI evaluation results in the training set reflect that incrementally adding parameters can optimize the model. Additionally, DCA demonstrated that the nomogram model provided significant clinical net benefits across both the training and test sets, indicating its robust utility in clinical decision-making (Fig. 5C and D). CIC analysis revealed that the nomogram model exhibited strong concordance between predicted values and actual clinical outcomes at higher risk thresholds, specifically when the risk threshold exceeded 0.7 in the training set and 0.4 in the test set, highlighting its reliability in practical clinical settings (Fig. 5E and F). Collectively, these findings underscore the efficacy of the nomogram model, which integrates both clinical and 3D-EIT parameters, demonstrating superior performance compared to models relying on single or limited parameters. Furthermore, the results suggest that 3D-EIT technology holds significant potential in aiding the identification of CTEPH.

Discussion

The clinical symptoms of CTEPH, such as chest tightness, palpitations, and reduced exercise capacity, are non-specific and often overlap with idiopathic pulmonary hypertension, making the diagnosis challenging. While right heart catheterization is used to measure pulmonary artery pressures, additional tests like V/Q scanning or CTPA are necessary to identify pulmonary perfusion defects. V/Q scanning is considered the primary method for assessing actual lung tissue perfusion dysfunction, whereas CTPA mainly evaluates vascular conditions. Although V/Q scanning and CTPA are accurate and essential for the differential diagnosis of CTEPH, there may be cases where patients cannot tolerate or afford these methods, and using them for follow-up assessments may further increase the burden on patients. Given that 3D-EIT can non-invasively and radiation-free capture whole-lung ventilation and perfusion at the bedside, we explored the diagnostic value of 3D-EIT for CTEPH, with the aim of expanding its application in pulmonary vascular diseases and providing potential for CTEPH differentiation and follow-up monitoring.

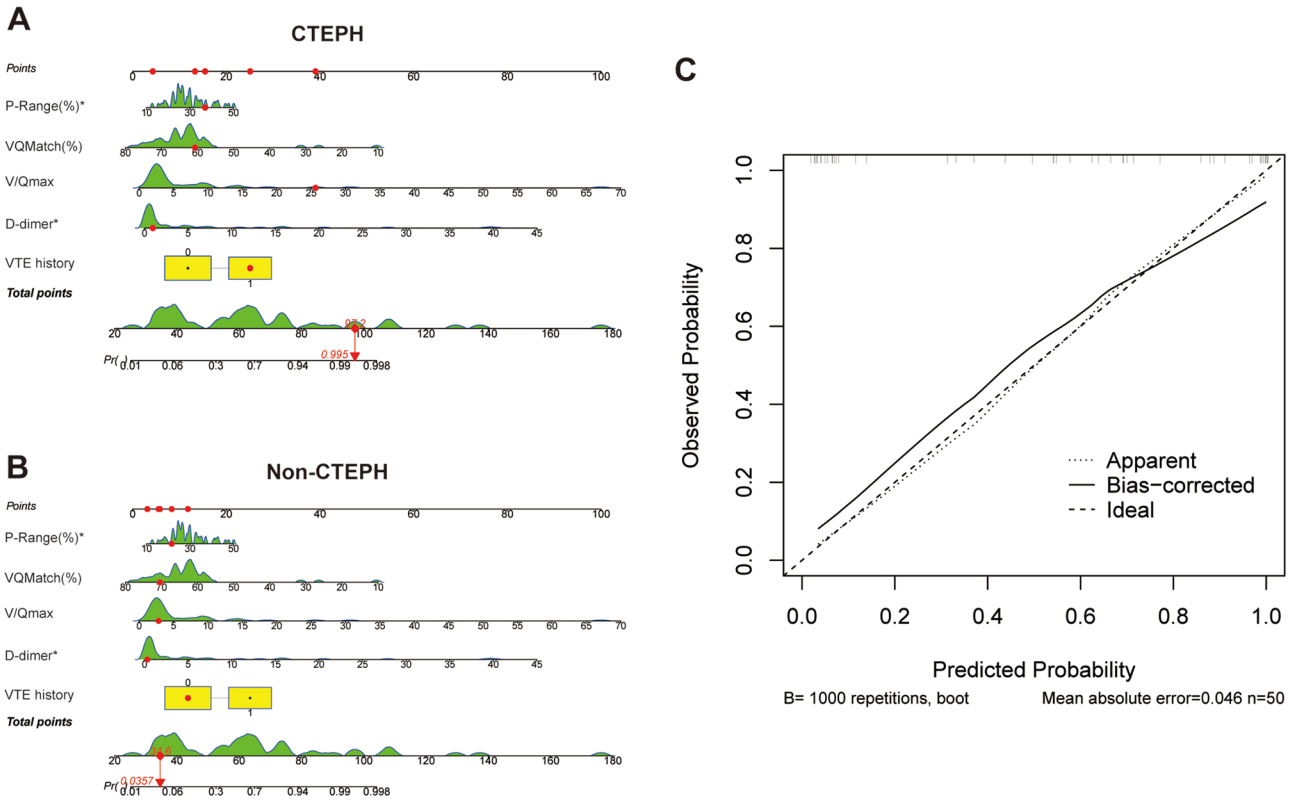

Fig. 4 Nomogram model and calibration analysis. (**A**) A typical nomogram diagnostic result in CTEPH patients. (**B**) A typical nomogram diagnostic result in Non-CTEPH patients. (**C**) Calibration curve analysis in the training set. Ideal represents perfect prediction. Apparent values represent apparent estimates of predicted and observed values. Bias-corrected values represent estimates corrected using 1000 bootstrap samples

In this study, we developed a diagnostic model for CTEPH by combining routine clinical data related to pulmonary hypertension and 3D-EIT parameters. Among the clinical factors, a history of PE, DVT or VTE status showed significant differences between CTEPH and Non-CTEPH patients, and VTE history was selected for the model. It is well established that CTEPH can result from a complication following an acute pulmonary embolism. The incidence of CTEPH appears to be approximately 2.3% among patients with acute pulmonary embolism [15]. Even in survivors who had received appropriate treatment, incomplete resolutions always put them at risk for developing CTEPH [16]. Our results also reflected this correlation. Although D-dimer reflects the presence of thrombus, its diagnostic significance for exclusion is greater when it is negative. In critically ill patients, D-dimer is not a reliable predictor for PE [17]. Previous studies found that D-dimer was insensitive and nonspecific for CTEPH diagnosis but was a significant predictor for the outcome of CTEPH [18, 19]. Therefore, additional research is required to explore the diagnostic and prognostic value of D-dimer in CTEPH. In this study, D-dimer was included in the model because it showed significant differences in the univariate analysis. Furthermore, various echocardiographic parameters (such as TRV max and mPAPe) did not show significant differences between the two groups. This aligns with previous international guidelines (ESC/ERS, 2022) and Chinese guidelines (2021), which suggest that echocardiography may primarily aid in distinguishing pulmonary hypertension caused by left heart disease. It is worth noting that the echocardiography-derived mPAP values in our study were higher than those obtained from RHC. Previous studies on different populations and varying severities of PH have shown that discrepancies between the two methods do exist, and the extent of these differences is closely related to the study context [20–23]. Since our research primarily focuses on the differential diagnosis of CTEPH rather than the diagnosis of PH itself, and there was no significant difference in the use of RHC for confirmation between the two groups, the potential bias introduced by this discrepancy is relatively small.

Several key parameters included in the model were derived from 3D-EIT. EIT detects changes in intrathoracic resistance, which reflect variations in lung gas volume and perfusion, and uses this information to reconstruct images of lung ventilation and perfusion. In the context of pulmonary vascular diseases, previous studies have shown that EIT, when combined with hypertonic saline bolus injection, can assist in diagnosing

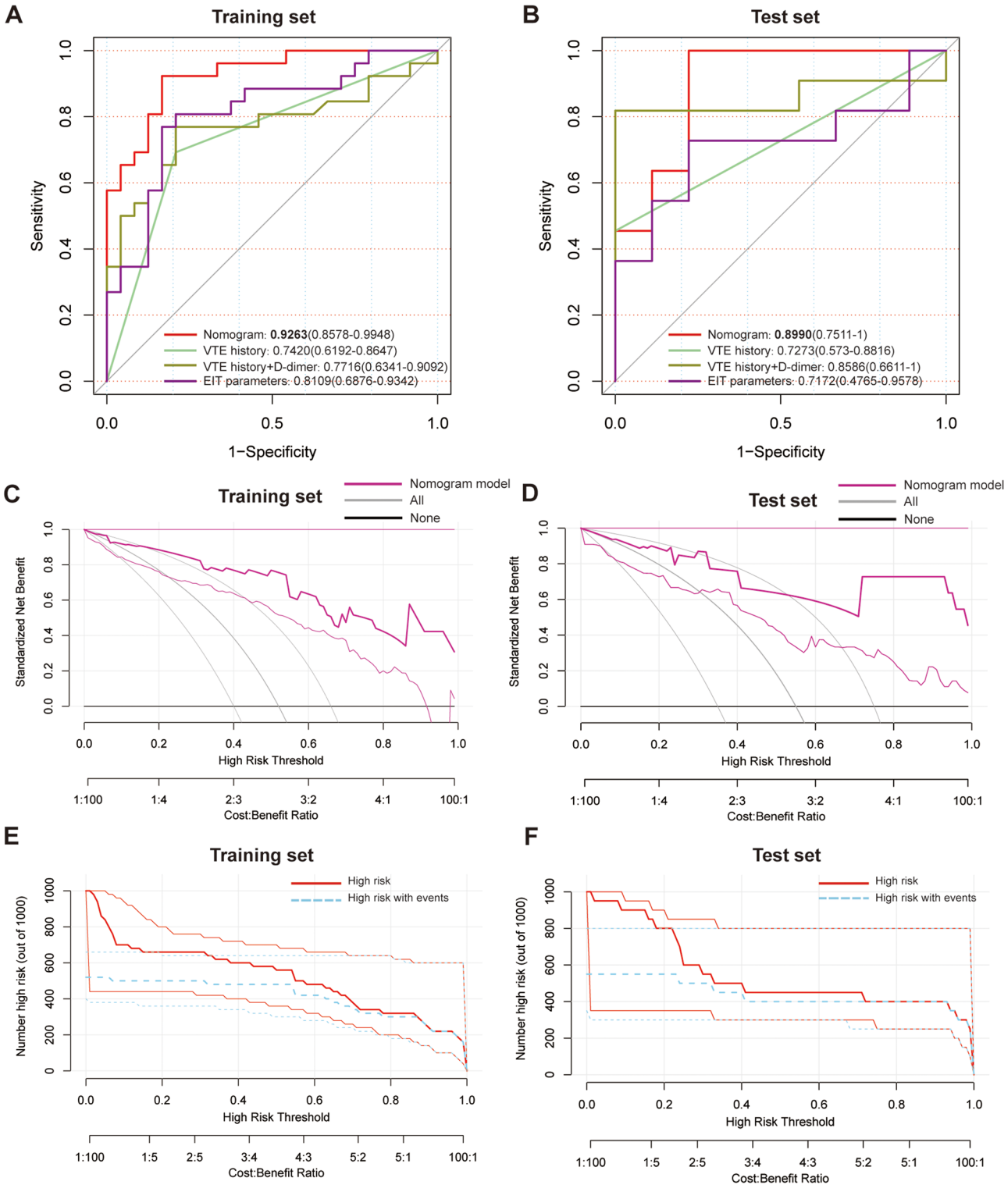

Fig. 5 ROC, DCA and CIC analysis of the nomogram model in the training and test datasets. (**A**) and (**B**) ROC evaluation of the nomogram model and the model incorporating partial parameters in the training and test sets. EIT parameters include V/Qmax, VQMatch and P-Range. (**C**) and (**D**) DCA evaluation of the nomogram model in the training and test sets. (**E**) and (**F**) CIC evaluation of the nomogram model in the training and test sets

pulmonary embolism at the bedside [24–26]. Additionally, EIT technology has been used to assess pulmonary pressure in healthy individuals exposed to normobaric hypoxemia [11]. These studies highlight the value of EIT perfusion imaging in the investigation of pulmonary vascular diseases. Our novel 3D-EIT technique, which utilizes a pulsatility-based algorithm instead of hypertonic saline injections combined with artificial breath-holding, broadens its potential applications. Additionally, the use of two electrode belts allows for the acquisition of whole-lung ventilation and perfusion signals, rather than just from a single level. These advancements enabled us to better characterize lung perfusion in patients suspected of having CTEPH. Theoretically, patients with CTEPH may exhibit localized perfusion deficits. In this study, CTEPH patients demonstrated a larger dead space area, a smaller VQMatch area, higher V/Qmax, and a greater range of regional perfusion values. These characteristics suggest that CTEPH patients experience significant heterogeneity in perfusion and a mismatch between ventilation and perfusion signals. The 3D-EIT findings were generally consistent with V/Q scanning, and three 3D-EIT parameters were included in the diagnostic model. Interestingly, the weak correlation between 3D-EIT and clinical parameters underscored the importance of constructing a model that integrates multiple parameters.

After performing univariate logistic analysis, Wald test, VIF, AIC and BIC evaluations, five variables (VTE history, D-dimer, V/Qmax, P-Range, and VQMatch) were incorporated into the nomogram model. The C-index (0.926, 95% CI: 0.859–0.993) and calibration analysis demonstrated that the model performed well. ROC and IDI analyses demonstrated that the stepwise inclusion of parameters can enhance the diagnostic performance of the model. DCA and CIC analyses demonstrated that the nomogram model offers substantial clinical net benefits, highlighting its practical utility in improving diagnostic accuracy and guiding clinical decision-making. These findings underscore the model's potential to enhance patient outcomes by providing reliable risk stratification and supporting tailored therapeutic strategies. Overall, the nomogram combining clinical and 3D-EIT parameters exhibited strong performance in diagnosing CTEPH.

The main strength of our study lies in enhancing the characterization of CTEPH and Non-CTEPH patients through 3D-EIT technology, and in constructing a comprehensive diagnostic model that integrates both clinical parameters and EIT data. However, a notable limitation of this study is the relatively small sample size, which may not fully represent the real clinical scenario and could hinder the robustness of model training and validation. Additionally, only a subset of patients (26 individuals) had RHC results, while the remaining patients were classified as having pulmonary hypertension based solely on echocardiography. Although RHC is the gold standard for diagnosing pulmonary hypertension, and there are certain discrepancies between echocardiography-derived and RHC-derived mPAP measurements, the acceptance of RHC did not significantly differ between the CTEPH and Non-CTEPH groups (Table 1). Furthermore, the baseline characteristics of patients who underwent RHC and those who did not were relatively consistent (Table S3). Therefore, the potential bias introduced by the absence of RHC is likely minimal. Despite this, our preliminary findings highlight the potential of 3D-EIT in CTEPH diagnosis and offer insights into developing easily accessible diagnostic and differential diagnostic models for CTEPH at the bedside. Future studies should aim to expand the cohort size, incorporate additional clinical features, and explore advanced 3D-EIT parameters to better capture the true perfusion characteristics of patients.

Conclusion

3D-EIT was first applied to identify the features of CTEPH, and a nomogram model was subsequently developed for CTEPH diagnosis, incorporating both clinical parameters (VTE history and D-dimer) and 3D-EIT parameters (V/Qmax, P-Range, and VQMatch). C-index and calibration analysis in the training set, along with ROC, DCA, and CIC analyses in the training and test set, demonstrated that this nomogram model exhibited strong diagnostic performance. 3D-EIT may provide future assistance in the identification and therapeutic evaluation of CTEPH.

Abbreviations

3D	Three-dimensional
AIC	Akaike information criterion
AUC	Area under the curve
BIC	Bayesian information criterion
CIC	Clinical impact curve
CO	Cardiac output
CTEPH	Chronic thromboembolic pulmonary hypertension
cTnT	Cardiac troponin T
DCA	Decision curve analysis
DeadSpace	Area of dead space detected by EIT
DVT	Deep venous thrombosis
EIT	Electrical impedance tomography
IDI	Integrated discrimination improvement
mPAP	mean right pulmonary artery pressure
mPAPe	mean right pulmonary artery pressure on echocardiography
NT-proBNP	N-terminal pro-brain natriuretic peptide
P, Q	Perfusion
PE	Pulmonary embolism
PH	Pulmonary hypertension
P-Range	Range between the maximum and minimum values of regional perfusion
RAD	Right atrial diameter
RHC	Right heart catheterization
ROC	Receiver operating characteristic curve
Shunt	Area of shunt detected by EIT
TRV	Tricuspid regurgitation velocity
V	Ventilation

V/Qmax	Maximum of corresponding regional ventilation/perfusion ratio
VIF	Variance inflation factor
VQMatch	Area with matched ventilation and perfusion on EIT
VTE	Venous thromboembolism

Supplementary Information

The online version contains supplementary material available at https://doi.org/10.1186/s12931-025-03206-9.

Supplementary Material 1

Acknowledgements
We appreciate the equipment and technical help provided by the Shanghai International Medical Science and Innovation Center-Excellence Innovation Center for Electromagnetic Medical Diagnosis and Treatment for this study.

Author contributions
XW, JX, YW, YG conceived this study. JX, YG and LW performed the EIT examination. JX and YW wrote the manuscript and designed the diagrams. YG edited the manuscript. XW and YS conducted and revised the paper. All authors read and approved the final manuscript.

Funding
This work was supported by Special Fund for Clinical Research of Zhongshan Hospital (ZSLCYJ202329), Shanghai Three-year Action Plan to Strengthen the Construction of Public Health System [GWVI-11.1-18]; The Construction of Multi-Disciplinary Treatment System for Severe Pneumonia [W2020-013]; Science and Technology Commission of Shanghai Municipality [grant number 20DZ2261200]; Data Sharing and Emulation of Clinical Trials[CCS-DASET，SHDC2024CRI043].

Data availability
Clinical and 3D-EIT data with personal information removed for data analysis can be obtained by contacting the corresponding author(s).

Declarations

Ethics approval and consent to participate
This study was approved by the ethics committee of Zhongshan Hospital (No. 402), and all participants provided written informed consent.

Consent for publication
Consent was obtained from the patient used to present the V/Q scanning and EIT images.

Competing interests
The authors declare no competing interests.

Author details
[1]Shanghai Key Laboratory of Lung Inflammation and Injury, Department of Pulmonary Medicine, Zhongshan Hospital Fudan University, Shanghai, China
[2]Shanghai Institute of Infectious Disease and Biosecurity, Fudan University, Shanghai, China
[3]Shanghai Respiratory Research Institute, Shanghai, China
[4]National and Shanghai Clinical Research Center for Aging and Medicine, Huashan Hospital, Fudan University, Shanghai, China
[5]Key Laboratory of Chemical Injury, Emergency and Critical Medicine of Shanghai Municipal Health Commission, Center of Emergency and Critical Medicine, Jinshan Hospital of Fudan University, Shanghai, China

Received: 25 October 2024 / Accepted: 27 March 2025
Published online: 12 April 2025

References

1. Delcroix M, Torbicki A, Gopalan D, Sitbon O, Klok FA, Lang I, Jenkins D, Kim NH, Humbert M, Jais X et al. ERS statement on chronic thromboembolic pulmonary hypertension. Eur Respir J. 2021;57.
2. Galiè N, Humbert M, Vachiery JL, Gibbs S, Lang I, Torbicki A, Simonneau G, Peacock A, Vonk Noordegraaf A, Beghetti M, et al. 2015 ESC/ERS guidelines for the diagnosis and treatment of pulmonary hypertension: the joint task force for the diagnosis and treatment of pulmonary hypertension of the European society of cardiology (ESC) and the European respiratory society (ERS): endorsed by: association for European paediatric and congenital cardiology (AEPC), international society for heart and lung transplantation (ISHLT). Eur Respir J. 2015;46:903–75.
3. Simonneau G, Torbicki A, Dorfmüller P, Kim N. The pathophysiology of chronic thromboembolic pulmonary hypertension. Eur Respir Rev. 2017;26.
4. Xu M, He H, Long Y. Lung perfusion assessment by bedside electrical impedance tomography in critically ill patients. Front Physiol. 2021;12:748724.
5. Frerichs I, Amato MB, van Kaam AH, Tingay DG, Zhao Z, Grychtol B, Bodenstein M, Gagnon H, Böhm SH, Teschner E, et al. Chest electrical impedance tomography examination, data analysis, terminology, clinical use and recommendations: consensus statement of the translational EIT development study group. Thorax. 2017;72:83–93.
6. He H, Chi Y, Long Y, Yuan S, Zhang R, Yang Y, Frerichs I, Möller K, Fu F, Zhao Z. Three broad classifications of acute respiratory failure etiologies based on regional ventilation and perfusion by electrical impedance tomography: a hypothesis-generating study. Ann Intensive Care. 2021;11:134.
7. Wang X, Zhao H, Cui N. The role of electrical impedance tomography for management of High-Risk pulmonary embolism in a postoperative patient. Front Med (Lausanne). 2021;8:773471.
8. Fossali T, Pavlovsky B, Ottolina D, Colombo R, Basile MC, Castelli A, Rech R, Borghi B, Ianniello A, Flor N, et al. Effects of prone position on lung recruitment and Ventilation-Perfusion matching in patients with COVID-19 acute respiratory distress syndrome: A combined CT scan/electrical impedance tomography study. Crit Care Med. 2022;50:723–32.
9. Jimenez JV, Weirauch AJ, Culter CA, Choi PJ, Hyzy RC. Electrical impedance tomography in acute respiratory distress syndrome management. Crit Care Med. 2022;50:1210–23.
10. Hovnanian ALD, Costa ELV, Hoette S, Fernandes C, Jardim CVP, Dias BA, Morinaga LTK, Amato MBP, Souza R. Electrical impedance tomography in pulmonary arterial hypertension. PLoS ONE. 2021;16:e0248214.
11. Proença M, Braun F, Lemay M, Solà J, Adler A, Riedel T, Messerli FH, Thiran JP, Rimoldi SF, Rexhaj E. Non-invasive pulmonary artery pressure Estimation by electrical impedance tomography in a controlled hypoxemia study in healthy subjects. Sci Rep. 2020;10:21462.
12. Putensen C, Hentze B, Muenster S, Muders T. Electrical impedance tomography for Cardio-Pulmonary monitoring. J Clin Med. 2019;8.
13. Hentze B, Muders T, Luepschen H, Maripuu E, Hedenstierna G, Putensen C, Walter M, Leonhardt S. Regional lung ventilation and perfusion by electrical impedance tomography compared to single-photon emission computed tomography. Physiol Meas. 2018;39:065004.
14. Zhang K, Wang L, Guo R, Lin ZC, Li MK, Yang F, Xu SH, Abubakar A. A deep generative Model-Integrated framework for 3-D Time-Difference electrical impedance tomography. IEEE Trans Instrum Meas. 2023;72.
15. Ende-Verhaar YM, Cannegieter SC, Vonk Noordegraaf A, Delcroix M, Pruszczyk P, Mairuhu AT, Huisman MV, Klok FA. Incidence of chronic thromboembolic pulmonary hypertension after acute pulmonary embolism: a contemporary view of the published literature. Eur Respir J. 2017;49.
16. Valerio L, Mavromanoli AC, Barco S, Abele C, Becker D, Bruch L, Ewert R, Faehling M, Fistera D, Gerhardt F, et al. Chronic thromboembolic pulmonary hypertension and impairment after pulmonary embolism: the FOCUS study. Eur Heart J. 2022;43:3387–98.
17. Sendama W, Musgrave KM. Decision-Making with D-Dimer in the diagnosis of pulmonary embolism. Am J Med. 2018;131:1438–43.
18. Arunthari V, Burger CD. Utility of d-dimer in the diagnosis of patients with chronic thromboembolic pulmonary hypertension. Open Respir Med J. 2009;3:85–9.
19. Skoro-Sajer N, Gerges C, Gerges M, Panzenböck A, Jakowitsch J, Kurz A, Taghavi S, Sadushi-Kolici R, Campean I, Klepetko W, et al. Usefulness of thrombosis and inflammation biomarkers in chronic thromboembolic pulmonary hypertension-sampling plasma and surgical specimens. J Heart Lung Transpl. 2018;37:1067–74.
20. Abu T, Levi A, Hasdai D, Kramer MR, Bental T, Bdolah-Abram T, Shiyovich A, Samara A, Vaknin-Assa H, Perl L, et al. Preoperative evaluation of pulmonary

hypertension in lung transplant candidates: echocardiography versus right heart catheterization. BMC Cardiovasc Disord. 2022;22:53.
21. Ciurzyński M, Bienias P, Ciesielska K, Chrzanowska A, Dudzik-Niewiadomska I, Kurnicka K, Domienik-Karłowicz J, Siwicka M, Sobieraj P, Kalińska-Bienias A, et al. Accuracy of doppler echocardiography in the hemodynamic assessment of pulmonary circulation in patients with systemic sclerosis. Adv Med Sci. 2019;64:309–14.
22. Kasai H, Matsumura A, Sugiura T, Shigeta A, Tanabe N, Yamamoto K, Miwa H, Ema R, Sakao S, Tatsumi K. Mean pulmonary artery pressure using echocardiography in chronic thromboembolic pulmonary hypertension. Circ J. 2016;80:1259–64.
23. Li J, Li A, Zhai Y, Li L, Zhang Y, Chen A, Tao X, Gao Q, Xie W, Zhai Z. Prevalence and risk prediction value of tricuspid regurgitation by echocardiography in precapillary pulmonary hypertension. BMC Pulm Med. 2022;22:409.
24. He H, Long Y, Frerichs I, Zhao Z. Detection of acute pulmonary embolism by electrical impedance tomography and saline bolus injection. Am J Respir Crit Care Med. 2020;202:881–2.
25. Grassi LG, Santiago R, Florio G, Berra L. Bedside evaluation of pulmonary embolism by electrical impedance tomography. Anesthesiology. 2020;132:896.
26. Yuan S, He H, Long Y, Chi Y, Frerichs I, Zhao Z. Rapid dynamic bedside assessment of pulmonary perfusion defect by electrical impedance tomography in a patient with acute massive pulmonary embolism. Pulm Circ. 2021;11:2045894020984043.

Publisher's note